*J. Fluid Mech.* (1980), *vol.* 99, *part* 3, *pp.* 469–479
*Printed in Great Britain*



# On laminar flow in curved semicircular ducts

By JACOB H. MASLIYAH
Department of Chemical Engineering,
University of Alberta, Edmonton, Canada

(Received 15 August 1979 and in revised form 28 November 1979)

Calculations of the flow field under laminar conditions in a helical semicircular duct have been made by numerically solving the Navier–Stokes equations. With the flat wall of the duct being the outer wall, the solution of the momentum equations for Dean numbers below 105 gave, for the secondary flow, twin counter-rotating vortices of Taylor–Goertler type. However, above a Dean number of $Dn = 105$, two solutions were possible. One solution was similar to that obtained for $Dn < 105$. The other solution revealed four vortices for the secondary flow. For $Dn > 105$, convergence to either flow pattern depended on the initial guess used in the numerical solution. Flow visualization confirmed the possibility of the presence of both types of secondary flow patterns.

## 1. Introduction

Laminar fluid flow in curved circular ducts has been studied both experimentally and theoretically (Dean 1928; McConalogue & Srivastava 1968; Itō 1969; Austin & Seader 1973; Collins & Dennis 1975; Van Dyke 1979). Laminar flow in circular ducts has been shown to be composed of a main flow along the curved duct axis with a superimposed secondary flow having twin counter-rotating vortices of Taylor–Goertler type.

For flow in helical square and rectangular ducts, having two sides of the duct walls parallel to the axis of rotation, Akiyama (1969), Cheng & Akiyama (1970) and Cheng, Liu & Ou (1976) observed that at high Dean numbers, depending on the initial guess of the flow field, their numerical solution gave either a two-vortex or a four-vortex flow pattern. They solved the momentum equations using a stream-function vorticity formulation with a point relaxation iterative numerical technique. Flow visualization confirmed the presence of a four-vortex flow pattern for a square duct (Cheng, Nakayama & Akiyama 1977).

Joseph, Smith & Adler (1975) solved the governing momentum equations in their primitive form for a square helical duct and noted the formation of a four-vortex flow pattern beyond a certain Dean number. However, no dual solution was reported. Also, they conducted flow visualization experiments confirming the presence of a four-vortex flow pattern. No photographs were published.

The experimental and numerical work of Humphrey, Taylor & Whitelaw (1977) on fluid flow in a 90 degree bent square duct indicated the presence of a two-vortex flow pattern only.

Collins & Dennis (1976*a*, *b*) numerically solved the fluid flow problem in a curved right-angled isosceles triangular tube with the hypotenuse being the outer wall and

0022-1120/80/4498-1600 $02.00 

parallel to the axis of rotation. Their work indicated the presence of a two-vortex flow pattern with a sequence of corner vortices of the type identified by Moffatt (1964). However, their numerical solutions did not reveal the formation of a four-vortex pattern. For a similar configuration, Collins & Dennis (1976*b*) gave a comparison of their results with a proposed asymptotic model as $Dn \to \infty$, due to Smith (1976).

The numerical work on fluid flow in semicircular helical ducts with the curved surface being the outer wall (Masliyah & Nandakumar 1979), did not reveal a four-vortex flow pattern. The usual two-vortex pattern was predicted. It appears then that the shape of the outer surface of a helical duct is important in determining the number of vortices of the secondary flow or at least it is easier to bring about the four-vortex pattern when the outer surface is flat. Using the previously developed numerical procedure of Masliyah & Nandakumar, the case of flow in a helical semicircular duct is studied with the flat surface being the outer wall.

In this communication, the term helical is used for bent ducts where the pitch of the helix is taken as zero.

## 2. Flow equations, boundary conditions and numerical procedure

The momentum equations in the stream-function vorticity form applicable to steady, fully developed incompressible laminar flow in a toroidal co-ordinate system $(r, \theta, \phi)$ are given by:

(i) axial component of Navier–Stokes equation

$$A_v v_\phi + B\frac{\partial v_\phi}{\partial \theta} + C\frac{\partial v_\phi}{\partial r} - \frac{\partial^2 v_\phi}{\partial r^2} - \frac{1}{r^2}\frac{\partial^2 v_\phi}{\partial \theta^2} = -\frac{Q}{H}; \tag{1}$$

(ii) vorticity-transport equation

$$A_\omega \omega_\phi + B\frac{\partial \omega_\phi}{\partial \theta} + C\frac{\partial \omega_\phi}{\partial r} - \frac{\partial^2 \omega_\phi}{\partial r^2} - \frac{1}{r^2}\frac{\partial^2 \omega_\phi}{\partial \theta^2} = D; \tag{2}$$

(iii) stream-function vorticity equation

$$\frac{1}{H}\frac{\partial^2 \psi}{\partial r^2} + \frac{1}{Hr^2}\frac{\partial^2 \psi}{\partial \theta^2} + \frac{\lambda}{rH^2}\frac{\partial \psi}{\partial r} - \frac{\cos\theta}{rH^2}\frac{\partial \psi}{\partial \theta} = \omega_\phi. \tag{3}$$

Here

$$A_v = \frac{1}{H^2}\left[1 - \left(\frac{\sin\theta}{r}\right)\frac{\partial \psi}{\partial \theta} + \cos\theta\frac{\partial \psi}{\partial r}\right], \tag{4}$$

$$A_\omega = \frac{1}{H^2}\left[1 - \cos\theta\frac{\partial \psi}{\partial r} + \frac{\sin\theta}{r}\frac{\partial \psi}{\partial \theta}\right], \tag{5}$$

$$B = \frac{1}{rH}\left[\frac{\partial \psi}{\partial r} - \cos\theta\right], \tag{6}$$

$$C = -\left[\frac{1}{r} + \frac{\sin\theta}{H} + \frac{1}{rH}\frac{\partial \psi}{\partial \theta}\right], \tag{7}$$

$$D = \frac{2v_\phi}{H}\left[\cos\theta\frac{\partial v_\phi}{\partial r} - \frac{\sin\theta}{r}\frac{\partial v_\phi}{\partial \theta}\right], \tag{8}$$

$$H = \lambda + r\sin\theta. \tag{9}$$

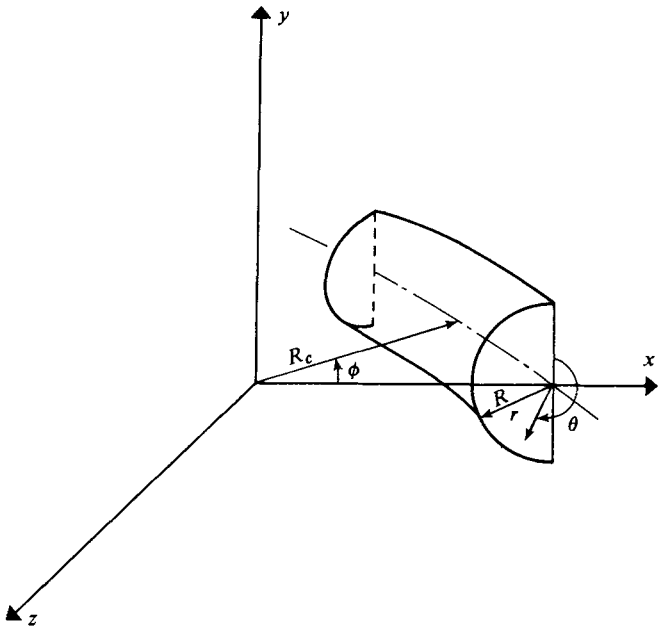


FIGURE 1. Co-ordinate system.

The flow equations were non-dimensionalized using $r = r'/R$, $\lambda = R_c/R$, $v_r = v_r'/(\nu/R)$, $v_\theta = v_\theta'/(\nu/R)$, $v_\phi = v_\phi'/(\nu/R)$, $\omega_\phi = \omega_\phi'/(\nu/R^2)$, $\psi = \psi'/(\nu R)$ and $Q = (\partial P'/\partial\phi)(R^2/\nu\mu)$. Here $Q$ represents the dimensionless pressure gradient, $\nu$ is the kinematic fluid viscosity, $\mu$ is the fluid viscosity, $\psi$ is the secondary-flow stream function, $\omega_\phi$ is the vorticity in the axial direction and $R_c$ is the radius of curvature. The prime denotes a dimensional quantity and $R$ is the radius of the duct.

The radial and angular velocities are given by

$$v_r = \frac{-1}{r(\lambda + r\sin\theta)}\frac{\partial\psi}{\partial\theta}, \tag{10}$$

$$v_\theta = \frac{1}{(\lambda + r\sin\theta)}\frac{\partial\psi}{\partial r}, \tag{11}$$

and the axial vorticity is given as

$$\omega_\phi = \frac{\partial v_\theta}{\partial r} + \frac{v_\theta}{r} - \frac{1}{r}\frac{\partial v_r}{\partial\theta}. \tag{12}$$

The stream function $\psi$ and the axial velocity, $v_\phi$, are taken as zero along the circular sector boundary. The vorticity along the curved surface is given by $(1/H)\,\partial^2\psi/\partial r^2$ and by $(1/Hr^2)\,\partial^2\psi/\partial\theta^2$ along the flat surface. Along $\theta = \frac{3}{2}\pi$, symmetry was assumed for the axial velocity and $\psi$ and $\omega$ are set to zero. The flow geometry is shown in figure 1.

The flow equations were solved using a second-order central-difference approximation. A relaxation technique was used in conjunction with the modified scheme of calculation as presented by Wilkes (1966), whereby two subgrids were used for each of the flow variables. This approach was proved to be twice as fast as the traditional successive over-relaxation (SOR) method. The details of the numerical technique are

given by Masliyah & Nandakumar (1977). Solutions were also obtained using the SOR method to ensure the validity of the numerical approach used in this study. The grid sizes used here are $\Delta\theta = \pi/30$ and $\Delta r = 0{\cdot}05$. Tests were conducted by reducing $\Delta\theta$ to $\pi/60$ and $\Delta r$ to 0·03333. For a Dean number of 150, the average velocity did not change by more than 0·5 %.

The validity of the numerical solution was further checked by integrating the wall shear stress $\tau_{r\phi}$ and $\tau_{\theta\phi}$ and equating the total shear force to the pressure force. The maximum deviation between the two quantities was 2 % for the coarse grid mesh.

In this analysis, the Reynolds and the Dean numbers are based on the equivalent diameter in order to be able to compare with other flow configurations. Defining a friction coefficient $C_f$ by

$$-\Delta p' A'_x = \tfrac{1}{2}\rho\langle v'_\phi\rangle^2 A'_s C_f \Delta\phi,$$

where $\Delta p'$ is the dimensional pressure drop, $\langle v'_\phi\rangle$ is the mean axial velocity, $A'_x$ is the cross-sectional flow area and $A'_s$ is the area, per unit $\phi$, on which the $\phi$-directed shear stress acts.

On putting $A_x = A'_x/R^2$ and $A_s = A'_s/R^2$, the friction coefficient is given by

$$C_f = \frac{-2QA_xD_e}{\langle v_\phi\rangle A_s Re},$$

where $Re = D'_e\langle v'_\phi\rangle/\nu = \langle v_\phi\rangle D_e$ and $D_e = D'_e/R = 4V'_w/A'_sR$. $V'_w$ is the dimensional wetted volume per unit $\phi$ and $D'_e$ is the dimensional equivalent diameter. For the flow geometry having the flat surface as the outer wall, then $A_x = \frac{1}{2}\pi$, $A_s = \lambda(\pi+2)-2$ and

$$D_e = \frac{4(\frac{1}{2}\lambda\pi - \frac{2}{3})}{\lambda(\pi+2)-2}.$$

The symbol $\lambda$ is the dimensionless radius of curvature, $R_c/R$. Utilizing the above definitions, the Dean number, $Dn$, becomes $Dn = Re/\lambda^{\frac{1}{2}}$. In the notation of Collins & Dennis and of Van Dyke, where $\kappa$ was used for Dean number, $Dn = \frac{1}{2}D_e\kappa$.

## 3. Flow visualization

The semicircular duct was constructed by first cutting a semicircular channel into the edge of a 21·5 cm diameter, 3·75 cm thick Plexiglas disk. A strip of thin Plexiglas was then glued around the edge of the disk to form the outer wall of the semicircular duct. For the viewing section, the disk was fitted with a Plexiglas block having straight outer edges as shown in figure 2. To minimize glare, the disk was blackened except for a 2 mm slit at the viewing plane. Two microscope light sources were used to illuminate a plane, along the slit, perpendicular to the main flow direction. Distilled water was used as the experimental fluid. The water was provided by a constant head tank.

Fluorescent ink (Hewlett–Packard Recorder Ink) was used to track the fluid. The ink was injected at the water inlet through a micro-syringe. Once the ink is at the illuminated plane, it fluoresces and changes colour from a very faint red to a bright green-yellow colour. As the very dilute ink has a very faint colour when not illuminated, it does not interfere with the viewing of the illuminated plane.

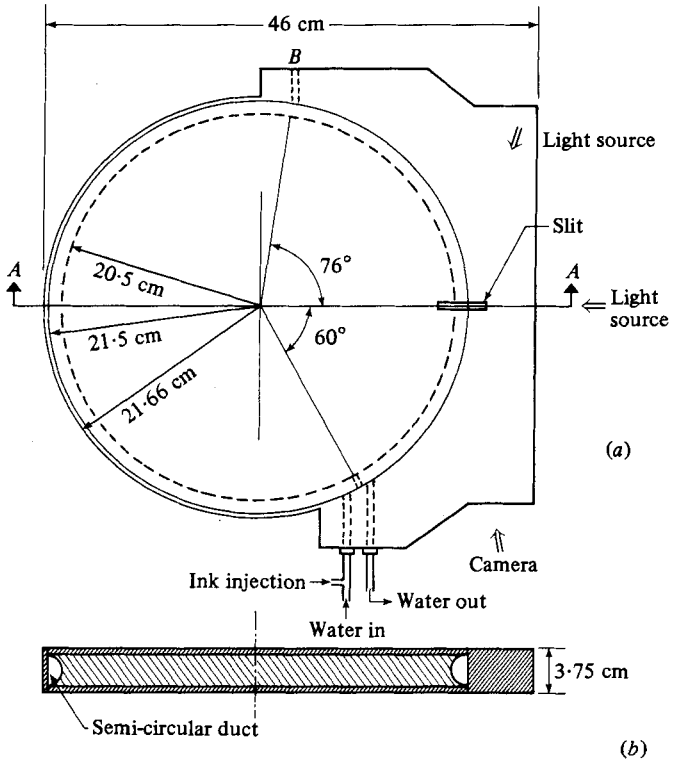


FIGURE 2. (*a*) Experimental set-up for flow visualization. (*b*) Section across $AA$.

The flow pattern was recorded using a camera with automatic winding mechanism fitted with a 50 mm Nikon macro lens. The exposure time varied from $\frac{1}{30}$ to $\frac{1}{4}$ second with a lens opening of $f4$ to $f11$.

## 4. Numerical results

The numerical approach used to obtain the flow field is an iterative one. For given $\lambda$ and $Q$, the flow field was evaluated in an iterative manner until a converged solution was obtained. Convergence was determined when the relative change of the velocity at each grid point was less than $10^{-4}$ between two consecutive iterations. Using the converged axial velocity, the average axial velocity $\langle v_\phi \rangle$ was then determined together with the friction coefficient and Dean number. For a given $\lambda$, solutions were obtained by progressively increasing or decreasing the pressure gradient $Q$.

When the value of the Dean number was less than 105, the flow-field solution converged to the same values regardless of the initial guess used and the solution exhibited a two-vortex flow pattern for the secondary flow. However, for $Dn > 105$, depending on the initial guess of the flow field, the numerical solution converged to either a two-vortex or a four-vortex flow pattern. One solution is that of the usual two-vortex flow pattern of Taylor–Goertler type. The other solution gives a four-vortex flow pattern where two additional vortices are attached to the Taylor–Goertler vortices.

The following example serves to illustrate the manner by which the initial guess

determines the type of solution obtained. Using an initial solution for $\lambda = \infty$, the flow field for $\lambda = 30$ and $Q = -0{\cdot}25 \times 10^6$ was obtained. The evaluated Dean number was 73·9 and a two-vortex flow pattern was predicted. Using the flow-field data for $Dn = 73{\cdot}9$ as the initial guess, a new solution for $\lambda = 30$ and $Q = -0{\cdot}7 \times 10^6$ was obtained having a Dean number of 159·4. This solution gave a four-vortex flow pattern. The converged results for $Dn = 159{\cdot}4$ were then used as the initial guess for $Q = -0{\cdot}5 \times 10^6$ and $\lambda = 30$. The converged solution gave a $Dn = 121{\cdot}9$ and it exhibited a four-vortex flow pattern. However, when the solution of $Q = -0{\cdot}25 \times 10^6$ ($Dn = 73{\cdot}9$) was used as the initial guess for $Q = -0{\cdot}5 \times 10^6$ and $\lambda = 30$, a two-vortex pattern was obtained having a $Dn = 131{\cdot}4$. In general, it was found that it is possible to maintain the type of the flow pattern of the initial guess as long as $Q$ is changed by a small amount.

Akiyama (1979) in his work on fluid flow in helical square channels found similar dependence on the initial guess of the flow field. However, Joseph *et al.* (1975), also working with square curved ducts, did not detect a dual solution and reported a two-vortex pattern for $Dn < 95$ and a four-vortex pattern for $Dn > 107$. The Dean number for the square duct is based on a Reynolds number with the equivalent diameter as the characteristic length and the radius of curvature normalized with half the square width.

Using flow visualization experiments, Joseph *et al.* reported a critical Dean number of 100, i.e. the minimum value of Dean number above which four-vortex flow pattern occurs. The numerical work on semicircular ducts of this study indicated that the critical Dean number is 105.

The dual solution exhibited by the momentum equations is not surprising because the equations are nonlinear and multiple solutions to hydrodynamic problems can exist. The presence of a dual solution to the present flow problem can be discussed within the framework of the theoretical and the experimental studies of Benjamin (1978*a*, *b*). In his work, Benjamin dealt with the case of flow problems that have more than one solution and the additional solutions arise from bifurcation at critical values of the flow parameters, namely Reynolds number. Benjamin defined two types of flows, (*a*) a primary mode which is that developed as Reynolds number is *gradually* increased from values where the flow is unique and (*b*) a secondary mode which is possible only above a certain critical value of Reynolds number. Benjamin reserved the term secondary mode for flows whose loci in a state diagram are disconnected from the locus of the primary mode and in which the secondary mode arises from one-sided bifurcation. The bifurcation point can be reached from above, i.e., once the secondary mode is established, the bifurcation point can be reached by slowly decreasing Reynolds number of the flow. Once the Reynolds number is less than the critical value, the secondary mode vanishes. Also, Benjamin stated that a secondary mode cannot be realized experimentally by gradually increasing the flow parameter but rather by a quick change in its value or by an 'experimental trick'.

The observations, due to Benjamin, described above were encountered in the numerical iterative procedure detailed earlier in this section. In the present study, the primary mode represents the two-vortex flow pattern and the secondary mode represents the four-vortex flow pattern. The primary mode was realized whenever a new solution was obtained from an initial guess having a not so different Dean number; provided that the initial guess is that of the primary mode. The secondary mode was

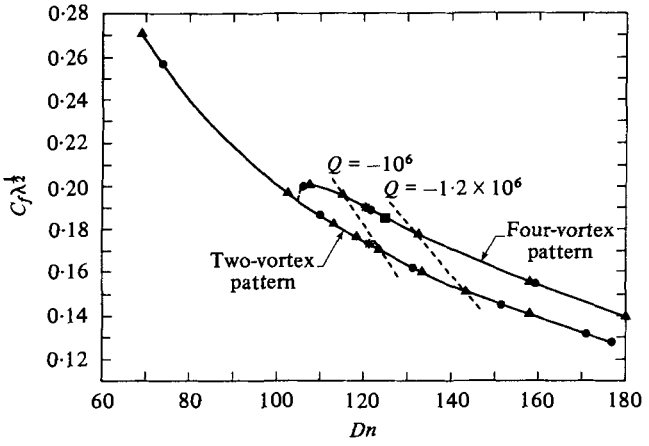


FIGURE 3. Variation of $C_f\lambda^{\frac{1}{2}}$ with Dean number. ★, $\lambda = 21{\cdot}5$; ●, $\lambda = 30$; ▲, $\lambda = 50$; ■, $\lambda = 1000$.

realized from a primary mode when the initial guess was of substantially different Dean number and the Dean number of the converged solution is above the critical value. The critical Dean number at which bifurcation occurs was obtained by gradually reducing the Dean number along the secondary mode until it merged with the primary mode, in a manner proposed by Benjamin.

Figure 3 represents a plot of a state function with a flow parameter. For this flow situation, the friction coefficient is taken as the state function discriminating amongst the different flows and the Dean number is the flow parameter. The exact location of the bifurcation point could not be established better than $Dn = 105 \mp 1$ as is shown in figure 3.

Figure 3 shows the variation of $C_f\lambda^{\frac{1}{2}}$ with Dean number. The plot indicates that for a given radius of curvature, $\lambda$, and a pressure gradient, $Q$, the average velocity as manifested by Dean number is higher for the case having a two-vortex flow pattern. This is not surprising, as more energy is likely to be dissipated in the four-vortex flow pattern. It is of interest to note that figure 3 is also similar to the well-known plot of torque coefficient, $C_M$, against Taylor number, $Ta$, for flow between two concentric cylinders (Schlichting 1968). In this plot, two curves for $C_M$ *versus* $Ta$ were obtained for the cases of laminar Couette flow and laminar flow with Taylor vortices.

The pressure–flow curve of figure 3 indicates that all the data points for the different values of the radius of curvature, $\lambda$, lie on a single (two-branched) curve. This indicates that for $\lambda$ as low as 21·5 the flow behaviour is that of large $\lambda$ limit. Consequently, the results presented here are applicable for only large $\lambda$ range.

The experimental work indicated that the flow becomes unstable at a Dean number of about 150. It is for this reason that the numerical work was not extended well above this value. However, a solution exhibiting a two-vortex flow pattern was still realized numerically for a Dean number as high as 200.

The secondary flow is illustrated in figure 4 for a radius of curvature of 21·5 and for a Dean number of 121 for the case of a two- and a four-vortex flow pattern. The contours of the stream function are normalized with the global maximum stream function,

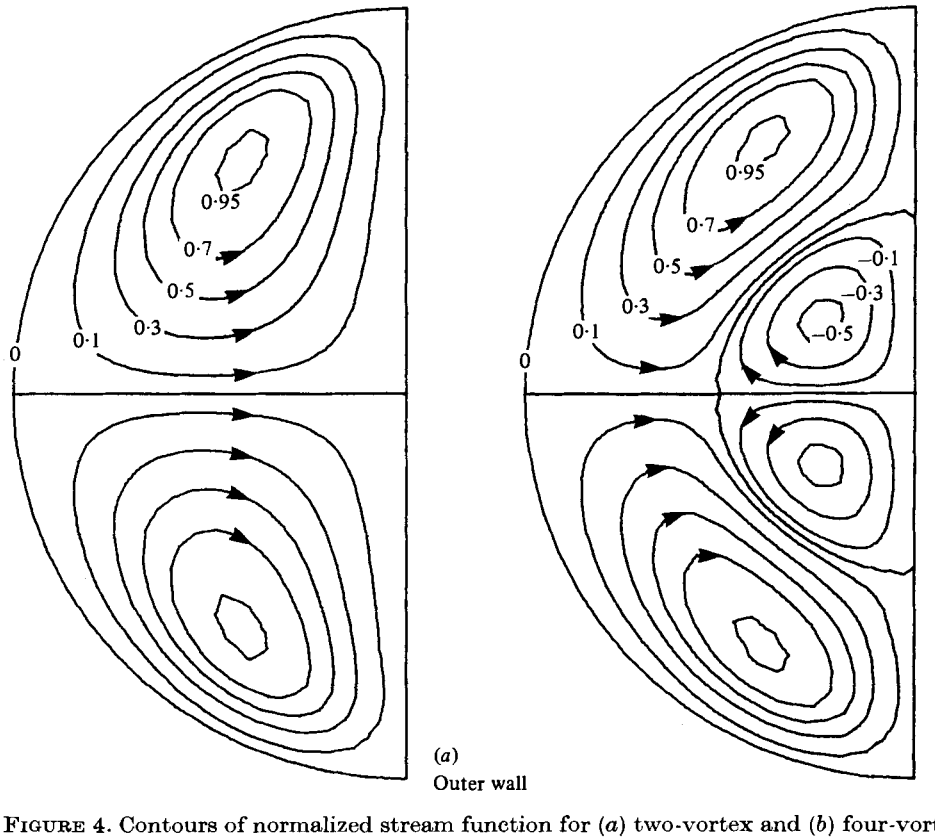


FIGURE 4. Contours of normalized stream function for (*a*) two-vortex and (*b*) four-vortex secondary flow patterns, $\psi/\psi_{max}$. (*a*) $\lambda = 21{\cdot}5$, $Q = -2{\cdot}74 \times 10^5$, $Dn = 121{\cdot}2$, $\psi_{max} = 172{\cdot}1$. (*b*) $\lambda = 21{\cdot}5$, $Q = -3{\cdot}01 \times 10^5$, $Dn = 121{\cdot}4$, $\psi_{max} = 159{\cdot}8$.

$\psi_{max}$, of the flow. The maximum value of the stream function of the secondary vortex is about one-half that of the primary vortex, indicating that the radial and the angular velocities in the secondary vortex are of the same order as those in the primary vortex. The primary vortex is referred to the vortex circulating close to the inner wall and the secondary vortex is that attached to the outer wall of the duct.

The effect of the presence of the secondary vortex on the normalized axial velocity is clearly seen in figure 5. When the secondary vortex is absent, the contours of equi-velocity lines are parallel to the outer wall and a boundary-layer-type flow is present for the entire wall. However, when the secondary vortex is present, the velocity contours indicate that fluid of lower velocity is carried towards the duct centre by the secondary vortex and a substantial distortion to the boundary layer at the outer wall occurs. For both the flow patterns the location of the maximum velocity no longer occurs at the duct centre but moves toward the duct corners. This feature is in agreement with the numerical results of Cheng & Akiyama (1970) and Collins & Dennis (1976*b*).

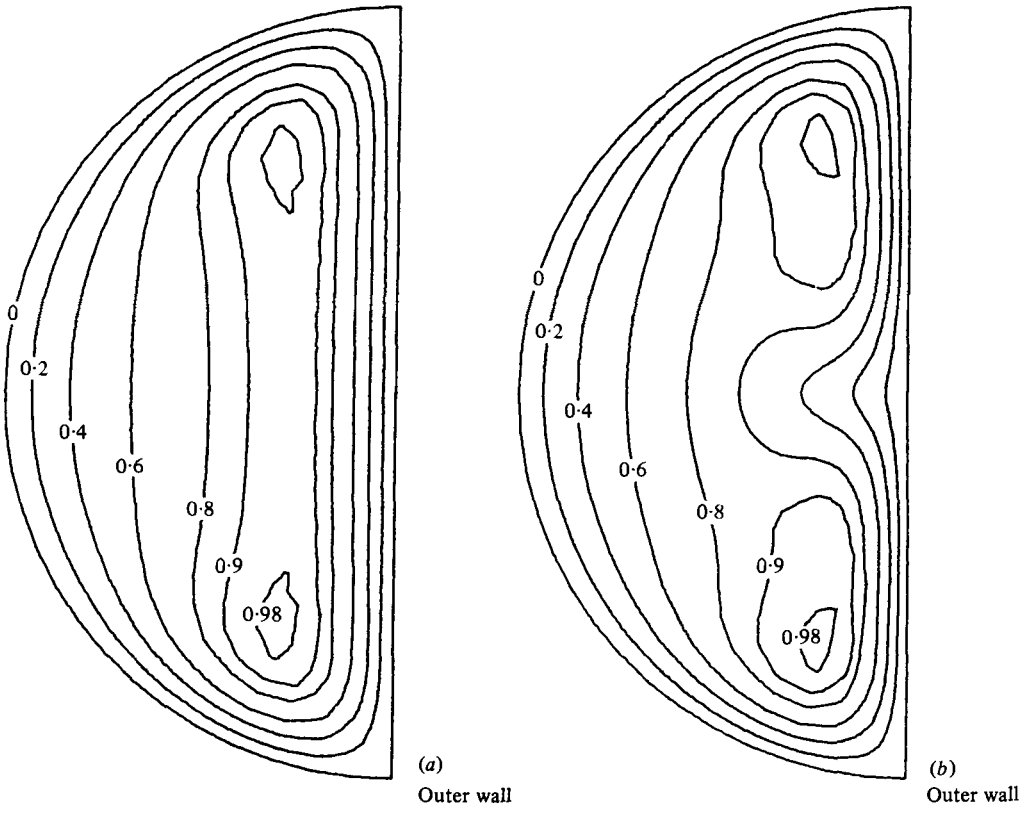


FIGURE 5. Contours of normalized axial velocity for (*a*) two-vortex and (*b*) four-vortex secondary flow patterns, $v_\phi/v_{\phi\,\max}$. (*a*) $\lambda = 21{\cdot}5$, $Q = -2{\cdot}74 \times 10^5$, $Dn = 121{\cdot}2$, $v_{\phi\,\max} = 779{\cdot}2$. (*b*) $\lambda = 21{\cdot}5$, $Q = -3{\cdot}01 \times 10^5$, $Dn = 121{\cdot}4$, $v_{\phi\,\max} = 778$.

## 5. Flow-visualization results

Flow-visualization experiments were conducted using the set-up of figure 2. The flow pattern due to the presence of the secondary flow was observed and photographed. For flow rates below a Dean number of about 150, the flow was found to be steady and only a two-vortex pattern was observed. However, on introducing a 0·8 mm diameter wire through port *B* into the flow duct, a four-vortex pattern emerged. The size of the secondary vortex was independent of the length of the wire protrusion in the duct as long as the protrusion is more than about half the duct radius. Photographs were taken with the wire fully inserted in the duct. When the Dean number was below 95, only a two-vortex flow pattern could be obtained, regardless of whether the wire protrusion is present or not. Figure 6 (plate 1) shows the two types of flow patterns, which are fairly similar to the predicted streamlines of figure 4.

When Dean number is higher than 150, flow oscillations were observed with and without the introduction of the wire disturbance. A typical flow pattern is shown in figure 7 (plate 2) for $Dn = 171$. Typical secondary vortex oscillation in the vertical plane with loss of symmetry can be observed.

Flow visualizations were also conducted with an arrangement similar to that of

figure 2 but with a semicircular duct having its curved circular surface as the outer wall. No four-vortex flow pattern could be detected for Dean numbers as high as 250. This is in agreement with the numerical work of Masliyah & Nandakumar (1979).

## 6. Concluding remarks

Numerical solution of the Navier–Stokes equations for fluid flow in a helical semicircular duct with its flat wall being the outer surface indicated that transition of the secondary flow pattern occurs at a critical Dean number of 105. Flow visualization experiments indicated a slightly lower critical Dean number of 95. Previous work on helical square ducts also indicated the presence of a flow pattern transition. The corresponding critical Dean number was about 100, which is fairly close to the value found in the work on semicircular ducts. Flow in ducts with a curved (circular) outer surface was not found to exhibit a transition in the secondary flow pattern. It appears that the shape of the outer surface is important in determining the transition and the pattern of the secondary flow. Work should be conducted to study the transition phenomenon of the flow pattern of the secondary flow in ducts with flat and curved outer surfaces.

The effect of the radius of curvature on the location of the bifurcation point, in other words, on the critical Dean number should also be studied for small values of the radius of curvature. In this manner, mapping regions for a dual solution can be determined and thereby a three-dimensional diagram for a state function, $C_f$, with a shape parameter, $\lambda$, and a flow parameter, $Dn$, can be established.

The author is indebted to the Natural Sciences and Engineering Research Council of Canada and the University of Alberta for financial support. The assistance in the experimental part of the work from Mr William Pick, Mr Helmut Schroeder and Mr John VanDoorn and encouragement from Professor S. C. R. Dennis are much appreciated.

## REFERENCES

AKIYAMA, M. 1979 Laminar convection in curved rectangular channels. M.Sc. thesis, University of Alberta.

AUSTIN, L. R. & SEADER, J. D. 1973 Fully developed viscous flow in coiled circular pipes. *A.I.Ch.E. J.* **19**, 85–94.

BENJAMIN, T. B. 1978*a* Bifurcation phenomena in steady flows of a viscous fluid. I. Theory. *Proc. Roy. Soc.* A **359**, 1–26.

BENJAMIN, T. B. 1978*b* Bifurcation phenomena in steady flows of a viscous fluid. II. Experiments. *Proc. Roy. Soc.* A **359**, 27–43.

CHENG, K. C. & AKIYAMA, M. 1970 Laminar forced convection heat transfer in curved rectangular channels. *Int. J. Heat Mass Transfer* **13**, 471–490.

CHENG, K. C., LIN, R.-C. & OU, J.-W. 1976 Fully developed laminar flow in curved rectangular channels. *Trans. A.S.M.E.* I, *J. Fluids Engng* **98**, 41–48.

CHENG, K. C., NAKAYAMA, J. & AKIYAMA, M. 1977 Effect of finite and infinite aspect ratios on flow patterns in curved rectangular channels. *Proc. Int. Symp. on Flow Visualization, Tokyo, Japan.*

COLLINS, W. M. & DENNIS, S. C. R. 1975 The steady motion of a viscous fluid in curved tube. *Quart. J. Mech. Appl. Math.* **28**, 133–156.

COLLINS, W. M. & DENNIS, S. C. R. 1976*a* Viscous eddies near a 90° and a 45° corner in flow through a curved tube of triangular cross-section. *J. Fluid Mech.* **76**, 417–432.

COLLINS, W. M. & DENNIS, S. C. R. 1976*b* Steady flow in a curved tube of triangular cross section. *Proc. Roy. Soc.* A **352**, 189–211.

DEAN, W. R. 1928 The stream-line motion of fluid in a curved pipe. *Phil. Mag.* **5** (7), 673–695.

HUMPHREY, J. A. C., TAYLOR, A. M. K. & WHITELAW, J. H. 1977 Laminar flow in a square duct of strong curvature. *J. Fluid Mech.* **83**, 509–527.

ITÖ, H. 1969 Laminar flow in curved pipes. *Z. angew. Math. Mech.* **11**, 653–663.

JOSEPH, B., SMITH, E. P. & ADLER, R. J. 1975 Numerical treatment of laminar flow in helically coiled tubes of square cross section. *A.I.Ch.E. J.* **21**, 965–974.

MASLIYAH, J. H. & NANDAKUMAR, K. 1977 Fluid flow and heat transfer in internally finned helical coils. *Can. J. Chem. Engng* **55**, 27–36.

MASLIYAH, J. H. & NANDAKUMAR, K. 1979 Fully developed viscous flow and heat transfer in curved semi-circular sectors. *A.I.Ch.E. J.* **25**, 478–487.

MOFFATT, H. K. 1964 Viscous and resistive eddies near a sharp corner. *J. Fluid Mech.* **18**, 1–18.

MCCONALOGUE, D. J. & SRIVASTAVA, R. S. 1968 Motion of a fluid in a curved tube. *Proc. Roy. Soc.* A **307**, 37–53.

SCHLICHTING, H. 1968 *Boundary-Layer Theory*, 6th edn, p. 503. McGraw-Hill.

SMITH, F. T. 1976 Steady motion within a curved pipe. *Proc. Roy. Soc.* A **347**, 345–370.

VAN DYKE, M. 1978 Extended Stokes series: Laminar flow through a loosely coiled pipe. *J. Fluid Mech.* **86**, 129–145.

WILKES, M. V. 1966 *A Short Introduction to Numerical Analysis*, p. 74. Cambridge University Press.

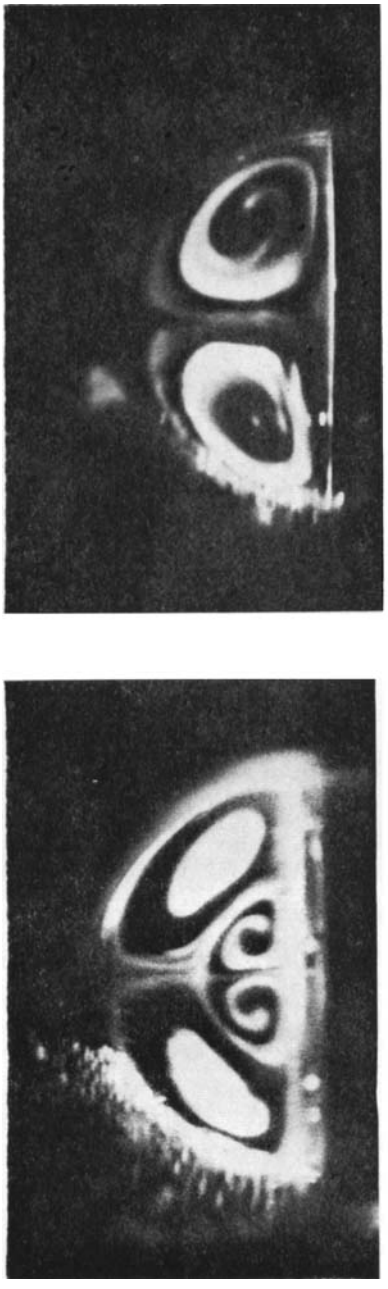


FIGURE 6. Secondary flow showing (*a*) two-vortex and (*b*) four-vortex flow patterns. $\lambda = 21{\cdot}5$, $Dn = 121$.

FIGURE 7. Secondary vortex oscillation for $Dn = 171$.